MECHANICAL BEHAVIOR OF THERMAL BARRIER COATINGS FOR GAS TURBINE BLADES*

Christopher C. Berndt ** , Woraphat Phucharoen and George C. Chang
Cleveland State University

ABSTRACT

Plasma-sprayed thermal barrier coatings (TBC's) will enable turbine components to operate at higher temperatures and lower cooling gas flow rates; thereby improving their efficiency. Future developments are limited by precise knowledge of the material properties and failure mechanisms of the coating system. Details of this nature are needed for realistic modelling of the coating system which will, in turn, promote advancements in coating technology.

The present work details complementary experiments and analytical modelling which has been undertaken in order to define and measure the important failure processes for plasma-sprayed coatings. The experimental portion includes two different tests which have been developed to measure coating properties. These are termed as "tensile adhesion" and "acoustic emission" tests. The analytical modelling section details a finite element method which was used to calculate the stress distribution in the coating system. Some preliminary results are presented.

1. INTRODUCTION

In the tensile adhesion test (TAT) a fixture is glued to the coating surface and the assembly subjected to a tensile force (ref. 1). The tensile strength of the coating is usually referred to as the bond strength. Two major criticisms of the TAT which are relevant to this work should be kept in mind. The forces imposed on the coating in a direction perpendicular to the substrate do not necessarily duplicate the forces which the coating experiences during its service life. Also the failure mode of the coatings, Fig. 1, cannot be controlled during a TAT and the coating will always fail at the weakest point under tension. This fracture mode may not be the same as failures experienced during the service life of the coating. In many cases mixed mode failure occurs and this makes it very difficult to exactly ascertain the failure mechanisms of coatings.

Thermally induced failure processes were also monitored during acoustic emission (AE) tests. The time and temperature dependent cracking processes gave rise to noise. Since failure of the thermal protection system is progressive then catastrophic failure occurs at some stage when there is a transformation from the microcrack to a macrocrack network.

The objective of the analytical work is to determine the distribution of stresses and strains for a model TBC system. Therefore the mechanical property measurements may be used in the analytical studies. These, in turn, will provide an

* Work performed under NASA/CSU cooperative agreement NCC3-27.
** Fellow of the Joint Institute for Aerospace Propulsion and Power.

understanding from the structural engineering viewpoint of the failure morphologies exhibited by coatings.

2. EXPERIMENTS

2.1 Tensile Adhesion Tests

The tensile adhesion tests were carried out on disc shaped specimens which were 32mm (1.25in) in diameter and 6mm (0.25in) in thickness with an edge radius of 3mm (0.125in). Thus the test surfaces of interest were 25.4mm (1.00in) in diameter and conformed to the ASTM standard test geometry (1). Bond coatings of NiCrAlY or NiCrAlZr were plasma-sprayed to a thickness of about 0.13mm (0.005in) at a power level of 13kW (450 amps and 29 volts). The ceramic overlay for all of the TAT specimens consisted of zirconia - 8wt% yttria which was plasma-sprayed at a power level of 17kW (550 amps and 31 volts) to an additional thickness of about 0.38mm (0.015in). These specimens will be identified as the Y bond coated and the Zr bond coated specimens.

The metal and ceramic deposits were approximately the same thickness over the entire specimen surface. This allowed the oxidative weight gain to be ascertained during preconditioning of the specimen by heat treatment. It should be noted that this study also examined batch variations during the processing of coatings. Thus the batch histories of the specimens are reported but they are not discussed in any detail.

The specimen was then incorporated into a tensile adhesion test configuration as depicted in Fig. 2 (ref. 2). It was necessary to include a collar into this arrangement, prior to specimen fabrication, so that tensile forces could be applied. Two pairs of knife edges were glued to the support bar and the collar so that extensometers could be attached to the specimen. These were in a back-to-back configuration and permitted the slightly non-axial forces imposed on the coating to be taken into account.

2.2 Thermal Cycling Tests

The specimens for the thermal cycling work consisted of 12.7mm (0.5in) diameter superalloy rods (U-700) which were plasma-spray coated over a length of 25mm near one end. The coating of 0.38mm (0.015in) zirconia - 12wt%yttria was sprayed either directly onto the substrate or onto 0.1mm (0.005in) of plasma-sprayed NiCrAlZr bond coat. Some poor coatings were also produced by spraying onto substrates which were preheated in excess of the optimum deposition temperature and these are termed as "preheated coatings". All specimens were cantilever supported so that they could be inserted into the hot zone of a tubular furnace.

The AE emitted from the sample was monitored during a heating and cooling cycle that ranged from 55^{o}C to 1200^{o}C. Most noise was emitted on cooling to below 550^{o}C. The threshold level of the AE equipment was adjusted by running calibration experiments so that no AE counts were evolved from oxidation of the substrate. The results which are reported here therefore measure AE processes which originate from the plasma-spray coating process. The AE (measured as either accumulative counts or count rate) was subsequently processed to reveal any trends dependent on temperature or coating process conditions.

2.3 Finite Element Modelling

The analytical modelling was also carried out on duplex coatings of 0.13mm (0.005in) bond coat with 0.38mm (0.015in) ceramic overlay. The coatings were assumed

to be applied to cylindrical specimens of 12.7mm (0.5in) in diameter and 76mm (3in) in length. The length to diameter ratio of the cylinder is sufficiently large that the numerical problem can be approximated by a two dimensional plain strain case. Figure 3 illustrates a slice of unit length from this cylinder which was considered for finite element analysis. The initial general approach to breaking up the unit slice into symetrical wedges is shown in figure 4. The interfacial region between the bond coat and ceramic coating was approximated by a sinusoidal function along the circumferential line where the radius is 6.48mm (0.255in), fig. 5. The peak-to-peak amplitude and period of this interfacial region was 0.05mm (0.002in). For the present study it has been assumed that the interface between the bond coat and substrate is smooth.

The three materials comprising the substrate, the bond coat, and the ceramic layer are treated as being homogeneous, isotropic, and linearly elastic. Each material possesses its own temperature dependent parameters, such as Young's modulus, Poisson's ratio, and thermal expansion coefficient. The values which were chosen for the preliminary analysis reported in this work are shown in Table 1. This simplified material model represents the first step towards obtaining a detailed solution to the complex TBC problem on hand. The finite element model paid attention to distinguishing elements in the vicinity of the sinusoidal interface. The only "load" applied to the model is one of uniform temperature and this simulates a temperature drop during the cooling cycle. The coating/substrate system was assumed to be stress free at 800^{o}, for the purposes of this work, and the stress was found after a 100^{o} drop.

Table 1. Material Data for Thermal Barrier Coatings.

	Substrate	Bond Coat	Ceramic Coating
Young's Modulus (GPa)	179.0	138.0	13.8
(psi x 10^{6})	25.5	20.0	2.0
Poisson's Ratio	0.25	0.27	0.25
Density (kg/m^{3})	37,590	33,830	27,390
(pci)	0.280	0.252	0.204
Thermal Expansion Coefficient ($m/m/^{o}C \times 10^{-6}$)	13.8	15.2	10.0
($in/in/^{o}F \times 10^{-6}$)	7.73	8.42	5.56

3. RESULTS

The change in tensile adhesion strengths with respect to oxidative weight gain are summarized in Fig. 6. All of the preoxidized Y and Zr bond coated specimens exhibited lower bond strengths than the as-sprayed Y bond coated specimens. The locus of failure was different for each sample preparation and coating system. The preoxidized Zr coated samples failed in a cohesive (C) manner, within the ceramic, whereas the as-sprayed Zr bond coated specimens exhibited failure at the substrate-bond coat interface (S). This adhesive type of failure within the as-sprayed coating is indicative of a poorly prepared coating. Nevertheless this bond strength value represents a minimum value of the cohesive mode which is observed during the service failure of coatings. On the other hand the Y bond coated samples did not exhibit either purely cohesive or any failure at the substrate-bond coat interface. All of

these preoxidized samples failed adhesively (A) whereas the as-sprayed coatings failed either adhesively or with a mixed mode A-C failure. Only one of these samples exhibited failure within the epoxy.

The Y bond coated specimens (Fig. 6a) revealed a general trend where the strength decreased with the specific weight gain. These failures also mostly incorporated an adhesive component. The bond strength results of Zr bond coated specimens (Fig. 6b) were ambiguous since the failure modes were not similar. The outlier of the Zr bond coated specimen (batch 1 as distinguished in Fig. 6) which exhibited the greatest weight gain also showed comparable bond strength to the other two preoxidized samples. The substrate interfacial-adhesive mode does not duplicate the cohesive failure mode experienced under service conditions. Therefore the values which have been obtained represent a minimum bond strength and the overall trend in bond strength may be to decrease with an increase in specific weight gain. The as-sprayed Y bond coated and preoxidized Zr bond coated samples most closely replicated the failure mode which was experienced in service.

The tensile tests measured the extension at two positions which were 180^{o} apart and thus the force versus average extension curve can be established. The average extension followed an approximately linear relationship with respect to the force until the failure point. Any fine detail on this curve has not yet been analysed. It was possible to calculate the compliance and elongation at fracture of these samples.

The AE tests indicated when cracking processes occurred within the specimen. Figure 7 shows the count rate data for the single component YSZ coatings. Acoustic emission is generated immediately upon cooling at $1200^{o}C$. This gradually decreases at a temperature of about $800^{o}C$. Acoustic emission signals are again generated at lower tempertures and the count rate increases to a maximum at approximately $100^{o}C$ before gradually decreasing to a temperature of $55^{o}C$. Then the next thermal cycle commences. For convenience this AE behavior is termed the "systematic response regime". In all cases there are small random fluctuations in the signal about the systematic trend. However in many cases there are also large erratic signals superimposed on the AE response curves. This AE behavior is referred to as the "stochastic response regime". These large count rates are thought to represent macro-cracking processes such as interlamellar cracking or coating delamination. They may also arise from prior-formed cracks which interact by sliding in a haphazard and irregular fashion. The processes which give rise to the systematic and stochastic regimes occur at higher temperatures for the preheated YSZ coating.

The duplex coating systems also exhibited the same trends. Examination of the first cycle (Fig. 8) shows that these coatings were less responsive, in terms of AE behavior, than the single component coatings which were examined above. The non-preheated coatings did not exhibit the stochastic noise distribution which was observed for the single component coatings. The non-preheated coatings commenced AE activity at temperatures less than $600^{o}C$ which may be compared to $1200^{o}C$ for all the other coating systems. The preheated duplex coatings displayed significant AE activity at temperatures greater than $1100^{o}C$. These samples also displayed more systematic and stochastic activity at temperatures less than $500^{o}C$ than the optimally sprayed duplex coating.

The second thermal cycle (not shown in this report) was different from the initial cycles. Both the systematic and stochastic distributions of AE increased and this resulted in a greater accumulative count. On the third cycle there was a further increase in the stochastic behavior so that the continuous behavior was

masked. It is difficult to discern real trends which may be associated with the initiation temperature of AE because these temperatures are all grouped within the 500-600°C temperature band.

The initial finite element calculations revealed that upon cooling compressive stresses developed in the ceramic parallel to the interface (in the Y direction) and mixed compressive and tensile stresses built up perpendicular to the interface (in the X direction). Shear stresses and the stresses in the X direction are localized near the interface (fig. 9). Stresses in the Y direction of the bond coat are compressive at the tips of the asperities and positive elsewhere. In the X direction the stresses are positive within the asperities and mixed elsewhere. Again shear stresses and the stresses in the X direction maximize near the bond coat - ceramic coating interface. It should be emphasized that these results are preliminary since these initial calculations have shown that a more refined mesh will be required in the vicinity of the interface.

4. DISCUSSION

The marked difference in failure mechanisms of the specimens makes comparison of the bond strengths difficult. It should be emphasized that the failure morphology which is observed during tensile adhesion testing does not always replicate the failure mode which is observed during furnace or burner rig tests. One other study (ref. 3) has examined the fracture modes of specimens in relation to the bond strength. It was found, in this earlier work, that bond strength increased as the locus of failure changed from the interface between the metal and ceramic to entirely within the coating. It is generally observed that the distribution of different modes of failure is not the same over the entire cross-sectional area of specimen. This may be explained in terms of different stresses and stress gradients across the specimen due to stress concentrations from a free edge (ref. 4). Other workers (ref. 5) have found difficulty in obtaining reproducible TAT data and several works (ref. 6,7) have proposed that tensile tests on notched bars may be used as a basis to obtain fracture mechanics values of coatings.

The Zr bond coated samples exhibited both a higher compliance and a greater net extension at failure than the Y bond coated specimens. The compliance, measured in mN^{-1}, can be considered as the reciprocal of the effective Young's modulus if the thickness of the coating (0.51mm or 0.020in) is also taken into account. Thus E = 1/(C x t) where E is Young's modulus, C the compliance and t is the thickness of both the bond and ceramic coatings. Therefore the average Young's modulus of the coating system measured in tension is in the range of 170 to 720 GPa. This is an over-simplification because deformation over the thickness of a duplex system would not be expected to be isotropic.

Coatings which exhibited the highest compliance (or lowest Young's modulus) may be expected to also reveal the greatest elongation at failure if it can be assumed that failure occurs by the same mechanism. However the failure mode is varied, being either adhesive, cohesive, substrate interfacial or of mixed mode. A few tentative relationships can be seen from the mechancial property determinations. The compliance of 75% of the Zr bond coated samples was greater than that of the Y bond coated samples. The average compliance of the Y bond coated specimens was 5.1×10^{-9} mN^{-1} whereas that of the Zr bond coated specimens was 8.3×10^{-9} mN^{-1}.

A number of experimental conditions should be remembered with regard to the acoustic emission tests. The heating and cooling rates of the specimen do not

represent practical operating conditions of a thermal barrier coating. However failure is still thought to occur on cooling in higher heat flux Mach 0.3 tests (ref. 8); and at higher heat fluxes, such as those in an engine, the cooling mode of failure is still likely to be important. Thus coating failure, for the present case, results from thermal expansion mismatch stresses between the coating and substrate as well as any oxidation effects of the bond coat and/or substrate.

The AE is assumed to correspond to cracking processes which occur as a result of the plasma-spray deposition process. Thus higher count rates, such as are observed from the stochastic regime, can be related to macrocracking processes and this has been supported by the observation of delamination during the first cycle for some specimens. Also the finite element studies indicate that the greatest stress build-up at the bond coat-ceramic coating interface most probably arises from shearing stresses.

Two different types of AE distributions can be observed by examining the count rate responses and both cracking processes are inter-related. The systematic response distribution is thought to represent the progressive growth and interaction of microcracks (i.e., subcritical crack growth) and possibly the spalling and interaction of oxidation products. The number of these events and their growth increases with decreasing temperature and therefore the AE count rate generation increases. The large count rates are presumed to evolve from uncontrolled macrocracking processes (i.e., critical crack growth). Thus macrocracking was observed to occur near the substrate-coating interace where stresses are greatest.

5. CONCLUDING REMARKS

A testing technique has been established which permits the properties of the coating only to be measured. The tensile properties of plasma-sprayed thermal barrier coating systems have been measured by a modified tensile adhesion test. The elongation at failure and the average compliance of the Zr bond coated specimens were both greater than those for the Y bond coated specimens. The average bond strength of the as-sprayed coatings was greater than that of the preoxidized specimens and this effect was most clear for the Y bond coated samples. Also the failure loci of the Y and Zr bond coated specimens were different.

The processing conditions, coating system structure (single versus duplex) and the number of thermal cycles influenced the AE response. The different cracking processes were distinguished by qualitative examination of the AE count rate data. The stochastic response, that is macrocracking processes, increased upon preheating of the coating and upon subjecting the specimen to increased thermal cycling. The stochastic response decreased when using a duplex coating instead of a single component coating.

Several experimental improvements can be offered in the light of the AE tests. The specimen geometry should permit 100% coverage of the plasma-sprayed coating system. In this manner AE events which arise from incomplete surface coverage, such as from edge effects, can be avoided. There is also the benefit that oxidative weight gains can be measured. Future tests shall control the furnace temperature gradient so that it is linear over the entire temperature range of experimentation. In this way temperature effects and change in temperature effects will not be confounded.

This work has been exploratory with the aim of using tensile adhesion test methods, AE techniques, and finite element modelling for examination of the

mechanical properties of plasma-sprayed coatings. It is anticipated that development of these methods can lead to a detailed understanding of the failure mechanisms and properties of coatings.

6. REFERENCES

1. ASTM, American Society for Testing and Materials,: "Standard C633-69 Method of Test for Adhesion or Cohesive Strength of Flame-Sprayed Coatings", (1969).
2. Berndt, C. C.; and Miller, R. A.: "Mechanical Property Measurements of Plasma-Sprayed Thermal Barrier Coatings Subjected to Oxidation", Ceram. Eng. Sci. Proc., Vol.5, (1984).
3. Levine, S. R.: "Adhesive/Cohesive Strength of a ZrO_2.12 w/o Y_2O_3/NiCrAlY Thermal Barrier Coating", NASA TM-73792, May 1978, 24 pages.
4. Sickfeld, J.: "Pull-Off Test, an Internationally Standardized Method for Adhesion Testing - Assessment of the Relevance of Test Results", in "Adhesion Aspects of Polymeric Coatings", pp.543-567, Ed. K.L.Mittal, Pub. Plenum Press, (1983).
5. Hermanek, E. S.: "Determining the Adhesive and Cohesive Strengths of Thin Thermally Sprayed Coatings", Welding J., 57 (1970) 31-35.
6. Pabst, R. F.; and Elssner, G.: "Adherence Properties of Metal-to-Ceramic Joints", J. Mater. Sci., 15 (1980) 188-196.
7. Berndt, C. C.: "Tensile Adhesion Test Measurements on Plasma-Sprayed Coatings", 6th. Inter. Conf. on Fracture, 4-10 Dec., 1984, New Delhi, India.
8. Miller, R. A.; and Lowell, C. E.: "Failure Mechanisms of Thermal Barrier Coatings Exposed to Elevated Temperatures", Thin Solid Films, 95 (1982) 265-273.

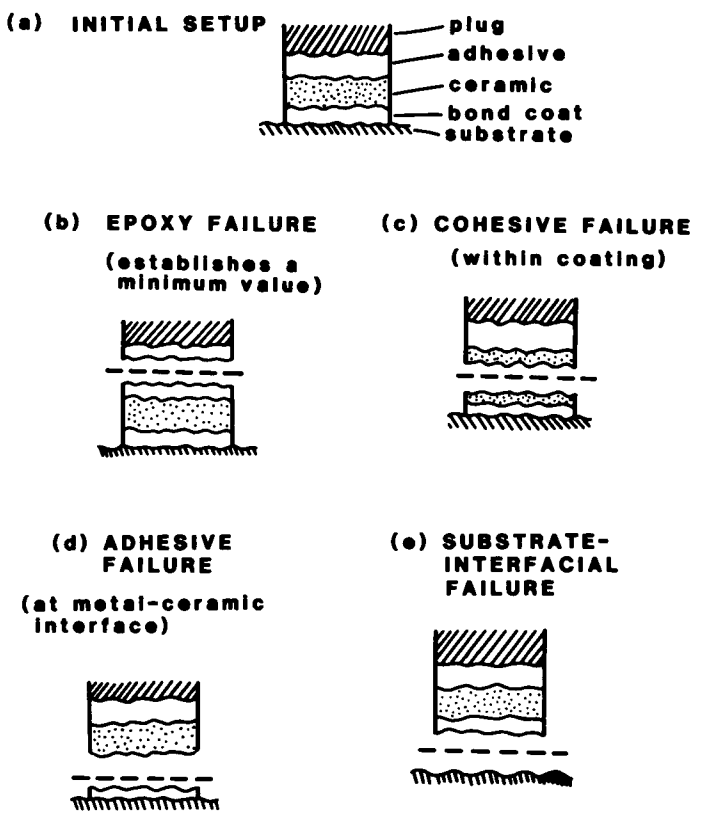

Figure 1. Modes of tensile adhesion test failures for plasma-sprayed coatings. Cohesive failure in the text is referred to as "C", adhesive failure as "A", and substrate-interfacial failure as "S".

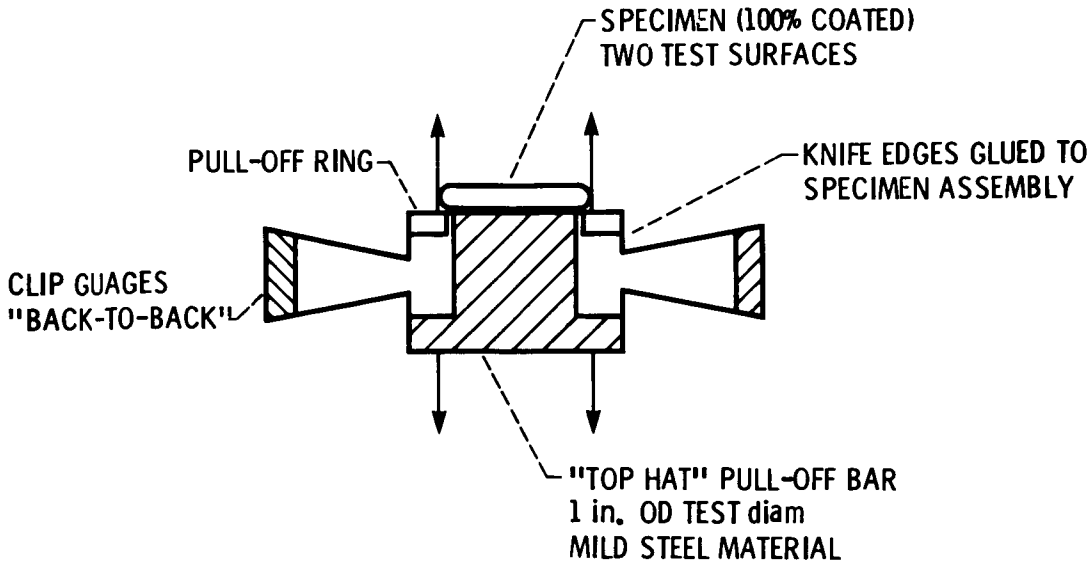

Figure 2. Specimen arrangement for carrying out tensile adhesion tests on plasma-sprayed coatings.

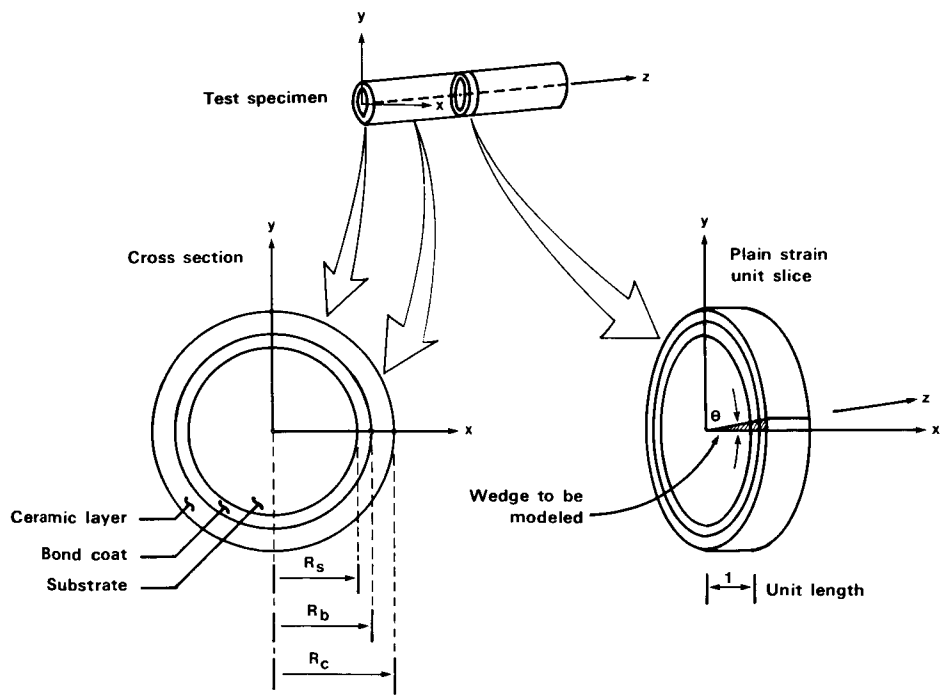

Figure 3. Cylindrical test specimen used for finite element modelling.

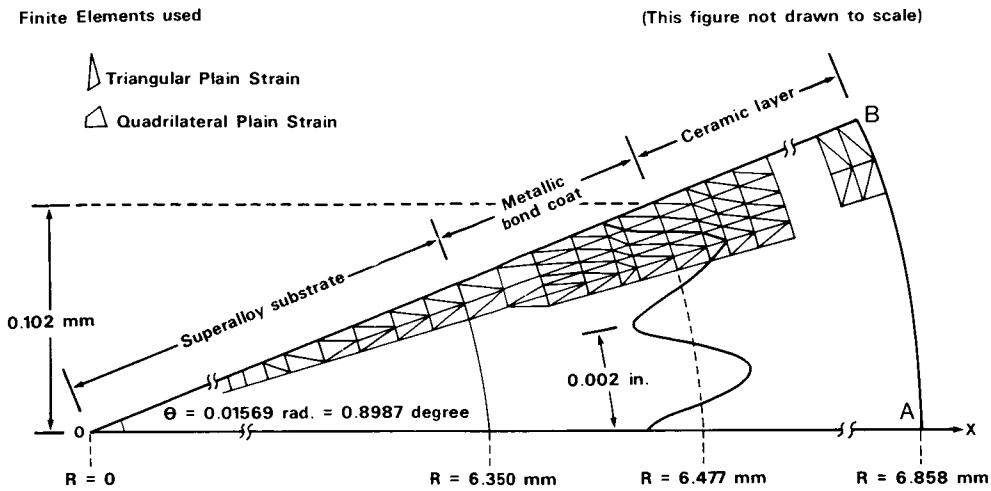

Figure 4. Schematic of the basic finite element model used for thermal barrier coatings.

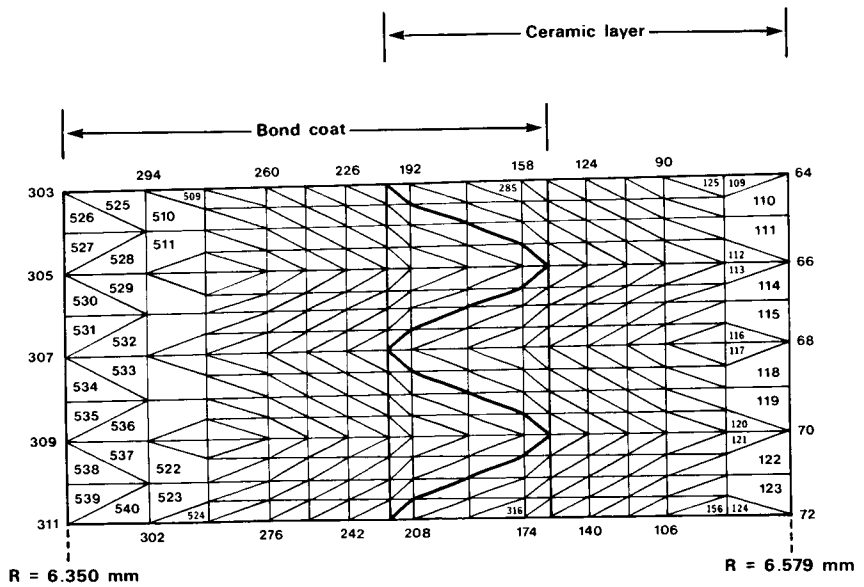

Figure 5. Details of the finite element model for thermal barrier coatings in the vicinity of the bond coat - ceramic coating interface.

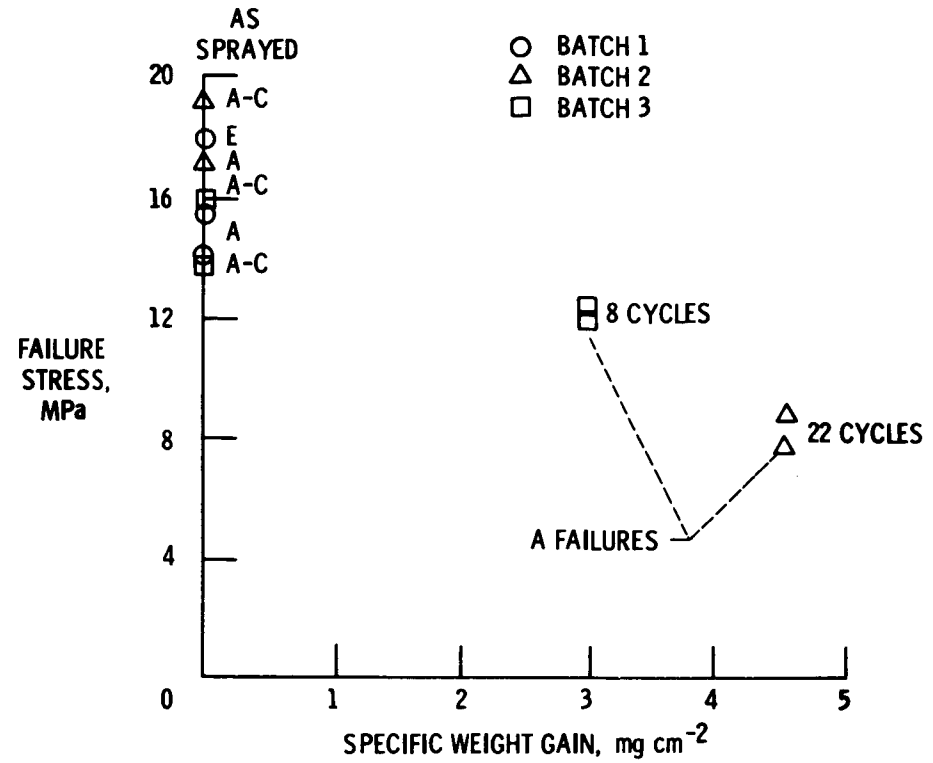

(a)

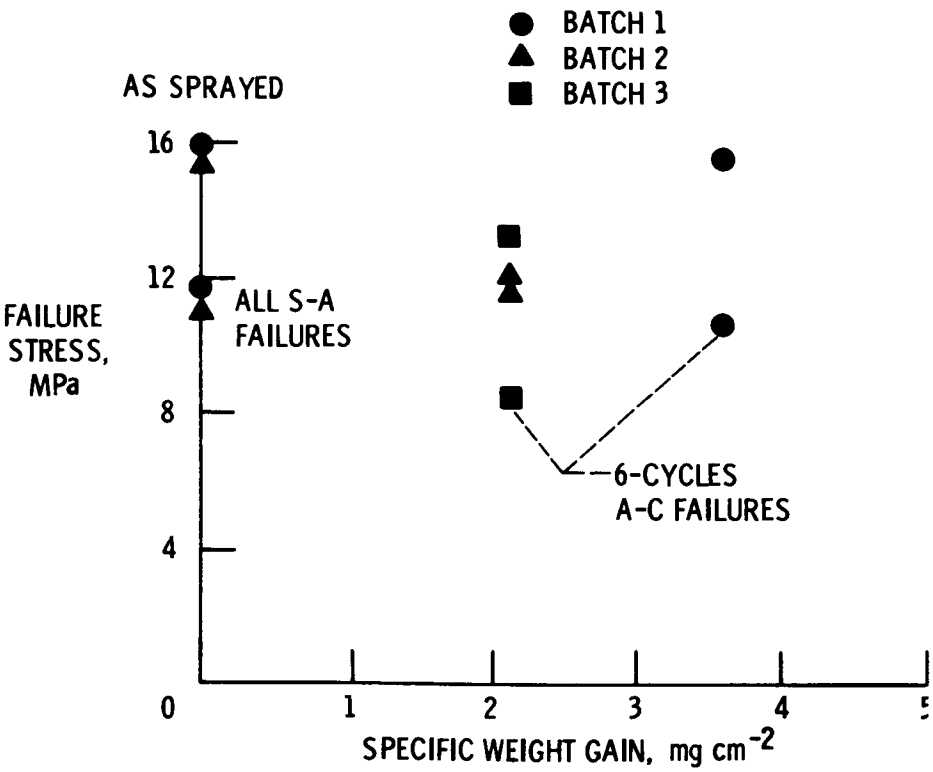

(b)

Figure 6. Bond strength of coatings with respect to specific oxidative weight gain. The modes of failure are also indicated.
(a) NiCrAlY bond coated. (b) NiCrAlZr bond coated.

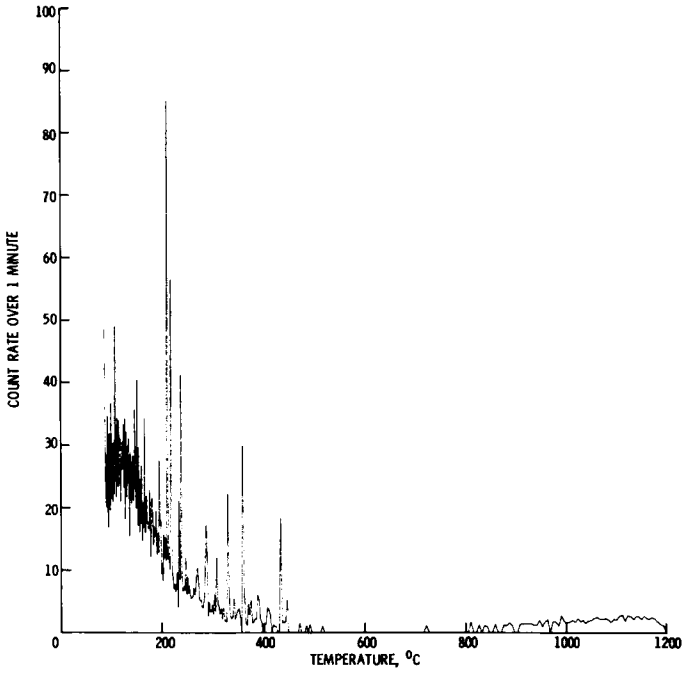

(a)

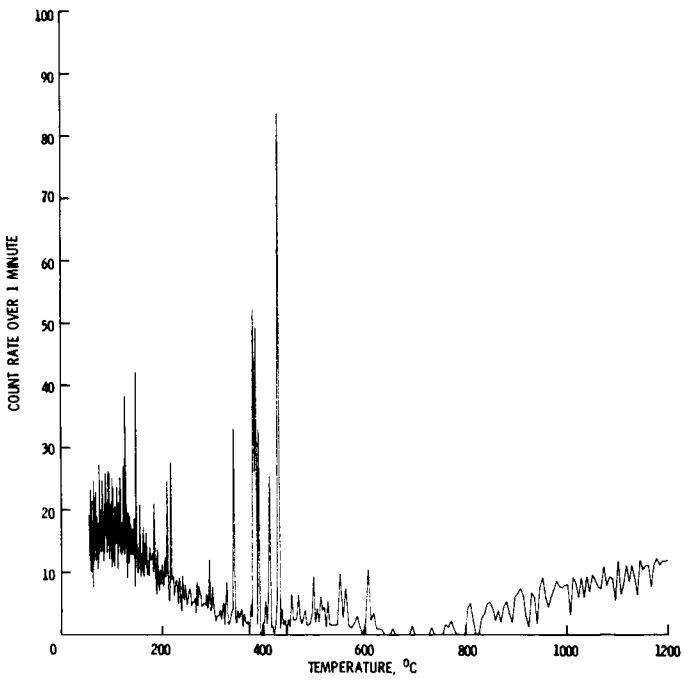

(b)

Figure 7. Acoustic emission response of single component coatings. (a) non-preheated coating. (b) preheated coating.

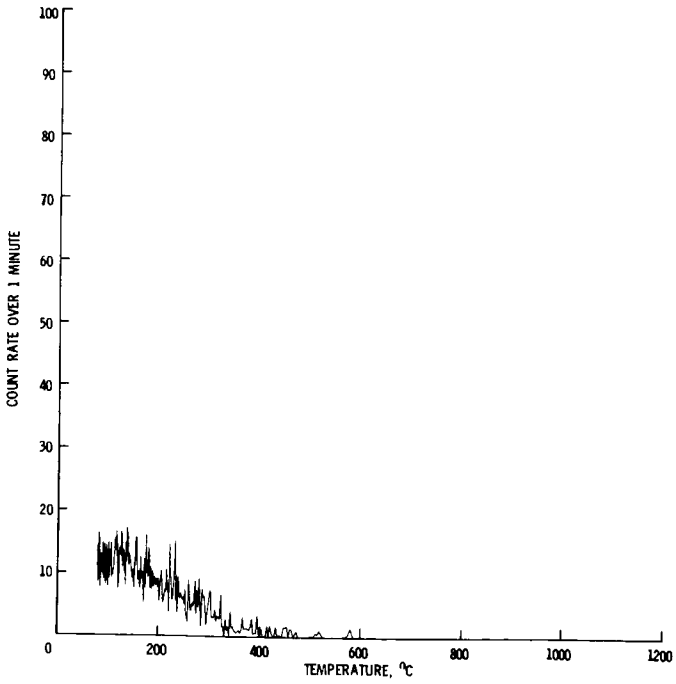

(a)

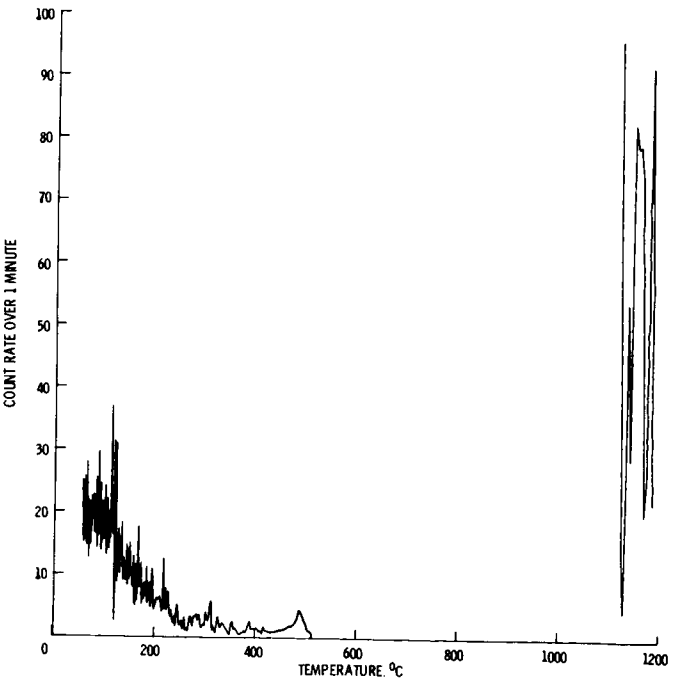

(b)

Figure 8. Acoustic emission response of duplex coatings. (a) nonpreheated coating. (b) preheated coating.

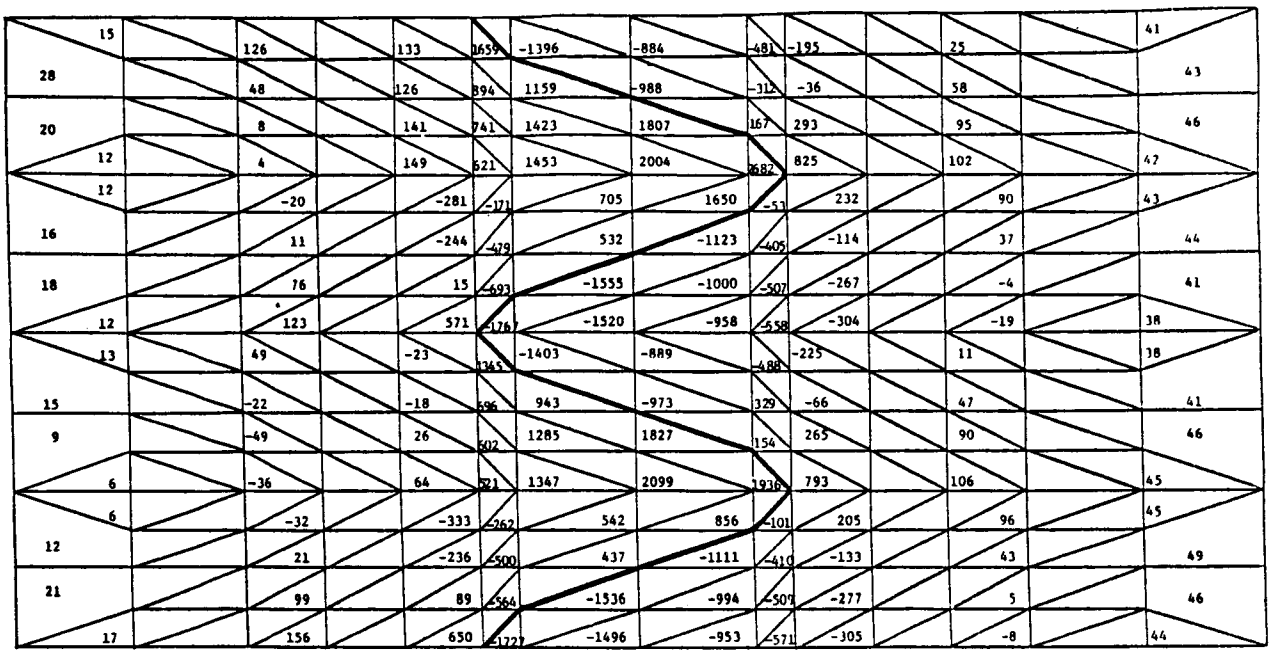

Figure 9a. Results from initial finite element modelling for the normal stresses in the X direction, refer to fig. 3. The numerical values are given in units of "psi". The bond coat is on the left hand side of the figure while the ceramic coating in on the right side.

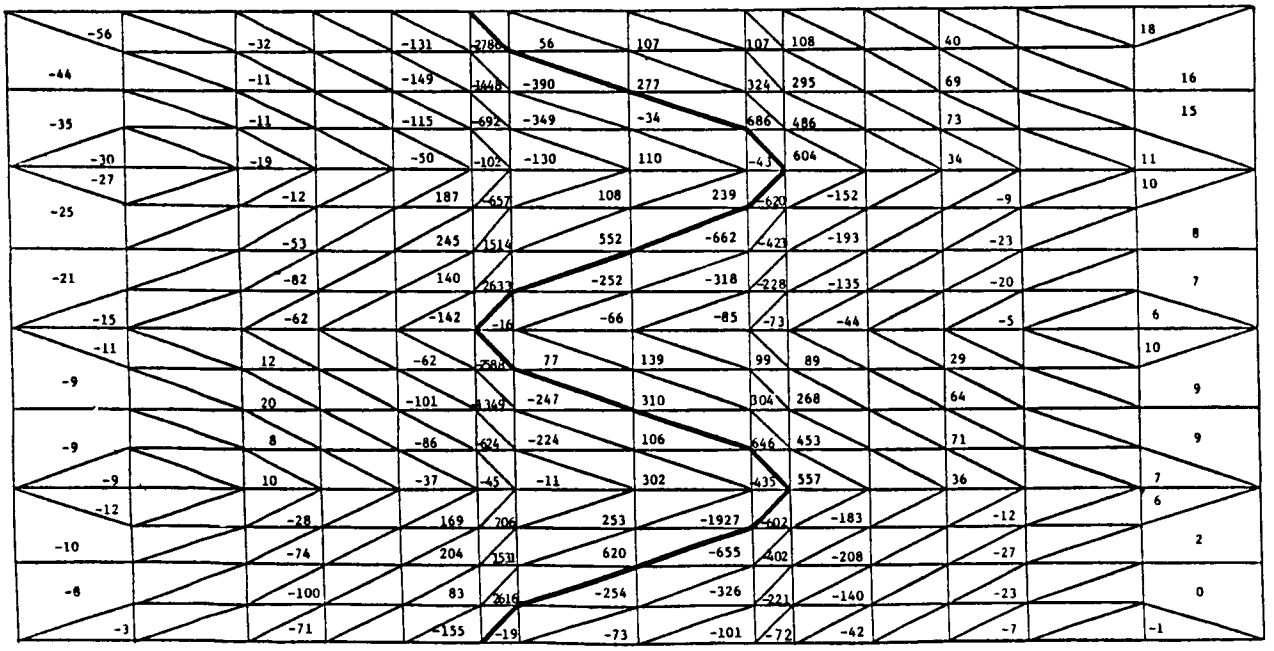

Figure 9b. Results from initial finite element modelling of the shearing stresses. The numerical values are given in units of "psi". The bond coat is on the left hand side of the figure while the ceramic coating is on the right hand side.